A Comparative Study of the H + FO ($v = 0, j = 0$) → (OH + F)/(HF + O) Reaction from QM and QCT Methods

T. S. Chu,*,† H. Zhang,‡ S. P. Yuan,† A. P. Fu,† H. Z. Si,† F. H. Tian,† and Y. B. Duan†

Institute for Computational Sciences and Engineering, Qingdao University, Shandong 266071, People's Republic of China, and Centre for Computational Molecular Science, Chemistry Building, The University of Queensland, Qld 4072, Brisbane, Australia

Received: January 9, 2009; Revised Manuscript Received: February 15, 2009

The dynamics of the title reaction are investigated using both the time-dependent quantum wave packet and the quasi-classical trajectory methods and employing a recently developed adiabatic ground $1^3A''$ potential energy surface [Gómez-Carrasco et al. *J. Chem. Phys.* **2004**, *121*, 4605]. By comparison to the quantum $J = 0$ reaction probabilities, the QCT method is first validated for the title reaction and further employed to produce the integral cross sections and rate constants. No resonance structures have been observed in both the QCT $J = 0$ and the quantum reaction probabilities of OH + F as well as in the QCT integral cross sections of both product channels, while there are some undulations in the calculated quantum reaction probabilities of HF + O. It is also found that Coriolis coupling effects play a significant role in the quantum calculation and that formation of the OH product is favored over the HF product in the reactive system.

1. Introduction

The OHF system has been given much attention in recent years. In 2004, Gómez-Carrasco et al.[1] performed high-level MRCI electronic structure calculations for 8069 energy points to calibrate the fitted potential energy surface (PES) of the ground adiabatic $1^3A''$ triplet electronic state. Starting from this high-quality triplet PES and a subsequent improved version,[2] quasi-classical trajectory (QCT) and wave packet studies[1−3] of $F(^2P) + OH(^2\Pi) \rightarrow O(^3P) + HF(^1\Sigma^+)$ and quantum state-to-state calculation[4] of the same reaction using a newly proposed coordinate transformation method in conjunction with the Coriolis-coupled (CC) method, photodetachment spectrum simulations[5] of OHF^-, and real wave packet state-to-state quantum dynamics study[6] of $H(^2S) + FO(^2\Pi) \rightarrow OH(^2\Pi) + F(^2P)$ have been carried out by Gómez-Carrasco et al., González-Sánchez et al., and Gogtas, respectively. In 2005, Gómez-Carrasco et al.[7] further reported the new PESs for the excited $2^3A''$ and $1^3A'$ triplet states and extended their previous dynamics study of the $F(^2P) + OH(^2\Pi) \rightarrow O(^3P) + HF(^1\Sigma^+)$ reaction by implementing wave packet calculations within the centrifugal sudden (CS) approximation on the excited triplet states, which also explored the possible contributions of the excited states and the nonadiabatic transitions to the reaction dynamics. As such, like many other reaction systems,[8,9] the OHF system can provide the opportunity to perform a nonadiabatic study with the coupled electronic states involved. The only set of coupled diabatic potential energy surfaces[10] of $1^3A''$, $2^3A''$, and $1^3A'$ has been developed and used in the calculations of the angular resolved photodetachment cross sections of OHF^- in 2006. Later, in 2007, the PESs[11] for the first five singlet states of the OHF system have been constructed from ab initio electronic structure calculations at the MRCI level for studying the photoelectron detachment processes of OHF^- at 213 nm. Of them, the ground adiabatic $1^1A'$ singlet PES is further employed in the subsequent quasi-classical trajectory and the wave packet calculations of $O(^1D) + HF(^1\Sigma^+) \rightarrow F(^2P) + OH(^2\Pi)$.[12] Therefore, various chemical processes including nonadiabatic processes could take place in the OHF reactive system, and it can be seen that the most studied process until now is $F(^2P) + OH(^2\Pi) \rightarrow O(^3P) + HF(^1\Sigma^+)$. The $F(^2P) + OH(^2\Pi)$ reaction can also lead to the formation of $H(^2S) + FO(^2\Pi)$, the theoretical dynamics investigations of which are however sparse, with only one quantum state-to-state dynamics calculation[6] of its reverse reaction being conducted very recently.

In this Article, we report a comparative dynamics study for the title reaction with both product channels of $OH(^2\Pi) + F(^2P)$ and $HF(^1\Sigma^+) + O(^3P)$ by performing a QCT calculation and a time-dependent quantum wave packet calculation with a split-operator scheme on the ground triplet $1^3A''$ PES. From quantum calculation, the converged total reaction probabilities for total angular momentum $J = 0$ have been obtained first. Next, reaction probabilities at several J values of 3, 5, 10, and 30 are calculated with the CS approximation. The role of Coriolis coupling effects in the quantum calculations has also been examined by comparing the $J = 3$ and $J = 30$ reaction probabilities generated from the CC and the CS calculations with and without Coriolis couplings. On the other hand, with two heavy atoms and with no permutational symmetry of the three atoms involved as well as with the potential well of the OHF system, quantum calculations of the title reaction have computational difficulty, so we therefore run QCT calculations on the same triplet surface. By comparing the $J = 0$ reaction probabilities from the quantum and the QCT calculations, we will show the validity of the QCT method in describing the dynamical behaviors of the title reactive system. Also, from a computational practical point of view, the QCT method is further used to calculate the integral cross sections for the two product channels at a number of fixed collision energies. After the calculated data of the integral cross sections were fitted, the initial state resolved thermal rate constants are further calculated by a Boltzmann averaging over the integral cross sections. This Article is structured as follows: Section 2 presents a brief

* Corresponding author. E-mail: tschu008@163.com.
† Qingdao University.
‡ The University of Queensland.

10.1021/jp9003505 CCC: $40.75
Published on Web 03/24/2009

description of the two dynamical methods, the QCT and the quantum mechanical (QM) time-dependent wave packet methods, followed by the calculated results and discussion in section 3.

2. QM and QCT Methods

In the present QM method,[13−16] the time-dependent Schrodinger equation for the H + FO reactive scattering problem is formulated within an adiabatic framework (only one PES of the $1^3A''$ triple state is involved) and with a reactant Jacobi coordinate $\{R,r,\theta\}$[14] being used throughout, and then it is solved by a split-operator scheme[17] where the time-independent Hamiltonian H is split into three parts, that is, the kinetic operator T_{trans}, the PES potential operator V, and the centrifugal potential operator V_{rot}, to act onto the wave functions $\psi(R,r,t)$ in each local representation space at each small time interval Δ. This process can be described using a formula language as follows:[13−16]

$$i\frac{\partial}{\partial t}\psi(R,r,t) = H\psi(R,r,t) = (T_{\text{trans}} + V_{\text{rot}} + V)\psi(R,r,t) \quad (2.1)$$

$$\psi(R,r,t+\Delta) = e^{-iH\Delta}\psi(R,r,t) = e^{-iT_{\text{trans}}\Delta/2}e^{-iV_{\text{rot}}\Delta/2}e^{-iV\Delta}e^{-iV_{\text{rot}}\Delta/2}e^{-iT_{\text{trans}}\Delta/2}\psi(R,r,t) \quad (2.2)$$

Here:

$$T_{\text{trans}} = -\frac{\hbar^1}{2\mu_R}\frac{\partial^2}{\partial R^2} - \frac{\hbar^1}{2\mu_r}\frac{\partial^2}{\partial r^2} + V(r) \quad (2.3)$$

$$V_{\text{rot}} = \frac{(\hat{J}-\hat{j})^2}{2\mu_R R^2} + \frac{\hat{j}^2}{2\mu_r r^2} \quad (2.4)$$

with $V(r)$ being the diatomic reference potential, and J and j being the total angular momentum and the diatomic rotational angular momentum.

Meanwhile, the wave function $\psi(R,r,t)$ is expanded within a basis set consisting of the translational basis function $u_n^v(R)$ and vibrational basis function $\phi_v(r)$ as well as the body-fixed-rotational basis function $Y_{jK}^{JM\varepsilon}(R,r)$:[13−16]

$$\psi(R,r,t) = \sum_{n,v,j,K} F_{nvjK}(t)u_n^v(R)\varphi_v(r)Y_{jK}^{JM\varepsilon}(R,r) \quad (2.5)$$

$u_n{}^v(R)$, $\phi_v(r)$ are the eigenfunctions of $-(\hbar^1)/(2\mu_R)(\partial^2)/(\partial R^2)$ and $-(\hbar^1)/(2\mu_r)(\partial^2)/(\partial r^2) + V(r)$ operators, and $Y_{jK}^{JM\varepsilon}(R,r)$ is the eigenfunction of (J^2,J_z,j^2,j_z). Specific forms of the basis functions can be found in refs 13 and 14. Fast Fourier transformation[18] and the discrete variable representation (DVR)[19,20] are used for the spatial coordinates to evaluate the action of the operators onto the wave function to improve the computational efficiency. Also, the operation of V_{rot} onto the rotational basis functions leads to Coriolis coupling effects due to that different K states coupled to each other via $((\hat{J}-\hat{j})^2)/(2\mu_R R^2)$; here, K denotes the projection quantum number of J and j.[21]

The initial value of this scattering problem is the $t = 0$ wave packet, which is constructed to describe the specified initial rovibrational state (v_0,j_0,k_0) of the diatomic reactant and to cover the investigated energy range. References 13−16 describe some details in constructing the initial wave packet, and here we shall not go further into this. Starting from the constructed $t = 0$ wave functions and iteratively applying eq 2.1 to the wave functions for quite long convergence time, the time-independent part of the final wave function, $\bar{F}_{nvjK}(E)$, which is calculated by a half Fourier transformation from the time-domain to the energy domain, is used to extract the initial state (v_0,j_0,k_0) selected reaction probability by carrying out the flux calculation at a fixed surface $r = r_s$:[13−16]

$$P_{v_0j_0k_0}^R(\mathrm{E}) = \frac{1}{\mu_r}\left(\sum_{n,v,j,K,v'} \bar{F}_{nvjK}^*(E)\varphi_v^*(\mathrm{r}) \times \frac{\partial}{\partial r}\varphi_{v'}(\mathrm{r})\bar{F}_{nv'jK}(\mathrm{E})\right)_{r=r_s}$$
$$\bar{F}_{nvjK}(\mathrm{E}) = \frac{1}{a(E)}\int_0^\infty e^{(i/\hbar)Et}\bar{F}_{nvjK}(\mathrm{t})\,\mathrm{dt}$$
$$\bar{F}_{nvjK}(t) = \sum_l A_{n,l}F_{lvjK}(t) \quad (2.6)$$

$A_{n,l} = \langle R_n|u_l^v(R)\rangle$ represents the transformation between basis and DVR representations along the R direction; see refs 13 and 14 for how to obtain $a(E)$. In addition, the Jacobi angle θ is used in the above calculation to distinguish between the two product channels with $0° \le \theta \le 90°$ and $90° < \theta \le 180°$, respectively.

The QCT calculations have been performed by the QCT code,[22−32] which includes the standard Monte Carlo sampling of the initial conditions, the integration of the Hamiltonian equation for nuclear motion, and the final assignment of the product rotational and vibrational quantum numbers. Here, we employed the symplectic integrator to solve the Hamiltonian motion equation.[32] Within this method, an integration step of 1 fs is found sufficient to ensure the total energy conservation and the total angular momentum conservation. The impact parameters are optimized, and after that batches of 250 000 trajectories are running on the ground triplet surface at a number of collision energies while setting the initial rovibrational conditions of the FO reactant to be $v = 0$, $j = 0$. The initial separation between the H atom and the FO molecule is chosen to be $18.9a_0$, and the maximum impact parameter is $5.7a_0$. The calculated and fitted QCT integral cross sections are employed in a Boltzmann averaging to obtain the temperature-dependent rate constant by applying the following equation:

$$k(T) = \sqrt{\frac{8k_BT}{\pi\mu_R}}(k_BT)^{-2}\int_0^\infty E\sigma(E)\exp\left(-\frac{E}{k_BT}\right)\mathrm{d}E \quad (2.7)$$

where k_B is the Boltzmann constant, E is the collision energy, and $\sigma(E)$ is the fitted QCT integral cross section.

3. Results and Discussion

In the time-dependent wave packet scattering calculation, the following parameters are found to be sufficient to converge the quantum calculation, the number of the grid points (the translational basis functions) in the R range from 0.02 to $15.5a_0$ is 160, including 120 grid points in the interaction range from 0.02 to $11.65a_0$, while in the r range of $0.5-11.0a_0$, 220 grid points are used with 190 and 8 vibrational basis functions for the interaction and asymptotic regions, respectively. A $j_{\max} = 120$ for rotational basis functions and a propagation time of 25 000 au are also used in the calculation. The flux analysis is performed at $r_s = 7.0a_0$. Figure 1 plotted the $J = 0$ total reaction probabilities versus the collision energy in the range of 0.2−1.0

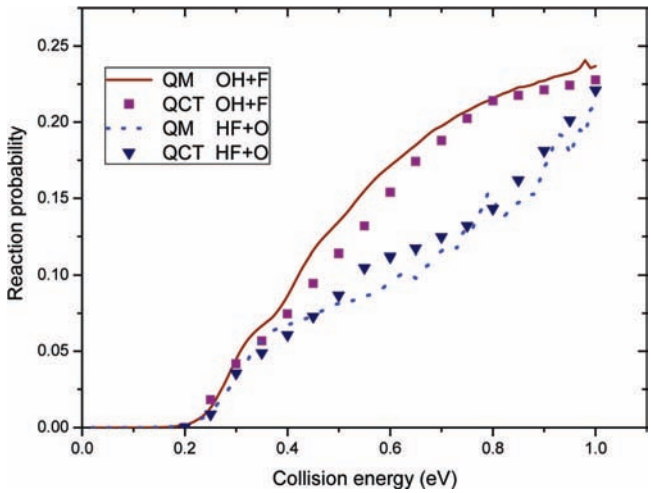

Figure 1. The calculated reaction probabilities for total angular momentum $J = 0$ as a function of collision energy over a range of 0.2−1.0 eV for the reaction of H + FO ($v = 0$, $j = 0$). The solid and dotted lines are quantum results for the OH + F and HF + O product channels, respectively. The corresponding QCT results are denoted, respectively, by the "■" and the "▼".

eV for H + FO ($v = 0$, $j = 0$) where the solid and the dotted lines correspond to the product arrangement OH + F and HF + O, respectively. As seen, the quantum reaction probabilities of both product channels show a reaction threshold of 0.2 eV and increase with the increasing collision energy. This threshold behavior is consistent with the energy barrier along the minimum energy path of the reaction system, which indicates a direct mechanism. Further, because the reaction is exoergic, that the two products exhibit the same threshold has nonetheless suggested that there exists an early barrier on the $1^3A''$ potential energy surface, as is shown in the collinear PES contours in Figure 2. There are almost no resonances in the $J = 0$ reaction probabilities of the OH + F product channel, while some oscillations can be observed in those of the HF + O channel, and the reaction probabilities of the OH + F channel are always larger than those of HF + O. In Figure 3, we present the quantum reaction probabilities for $J = 3$, 5, 10, and 30 for the two product channels, generated from the CS calculations that neglect Coriolis coupling effects. It can be seen that oscillations persist in the HF + O reaction probabilities for these individual J values, while there are still no resonances in the OH + F probabilities. Because the potential well is responsible for the appearance of the resonances in the reaction probabilities, this phenomenon has suggested that the presence of the potential well in the system could influence more the HF + O channel than the OH + F channel. Besides, the J-dependent behavior of OH + F is found to be quite different from that of HF + O, where a decreasing tendency with increasing J has been observed. We further examine the role of Coriolis coupling effects in the present quantum scattering calculation by comparing the CS reaction probabilities to those CC ones for $J = 3$ and $J = 30$. In the CC calculations, all possible quantum projections have been included in the $J = 3$ calculation, while the number of K used in the $J = 30$ calculation is 5. This comparison in Figure 4 shows that, for the HF + O product channel, the CS approximation underestimates the $J = 3$ and $J = 30$ reaction probabilities, and there are less pronounced resonances (no resonances) in the CC reaction probabilities for $J = 3$ ($J = 30$) due to further cancelation of the resonances by including K-block couplings. However, for the OH + F channel, the CS approximation is seen to overestimate the $J = 3$ and $J = 30$ reaction probabilities at high collision energies. Such pronounced Coriolis coupling effects are predictable because the large rotational constant of the heavy diatomic reactant FO of the title reaction implies strong Coriolis interactions. Furthermore, in a previous calculation[2] on the OH + F → HF + O reaction using the same triplet PES, it was found that QM calculation with the CS approximation agrees with the QCT calculation at higher collision energies where the direct mechanism dominates, while the two methods disagree for low energy scattering cases where resonances exist.[2] Hence, it is very likely that the failure of the CS approximation in the present quantum calculation is caused by the fact that the H to OF center of mass distance is far from being close to any inertia axes. Meanwhile, in performing the quantum calculations, we also noticed that

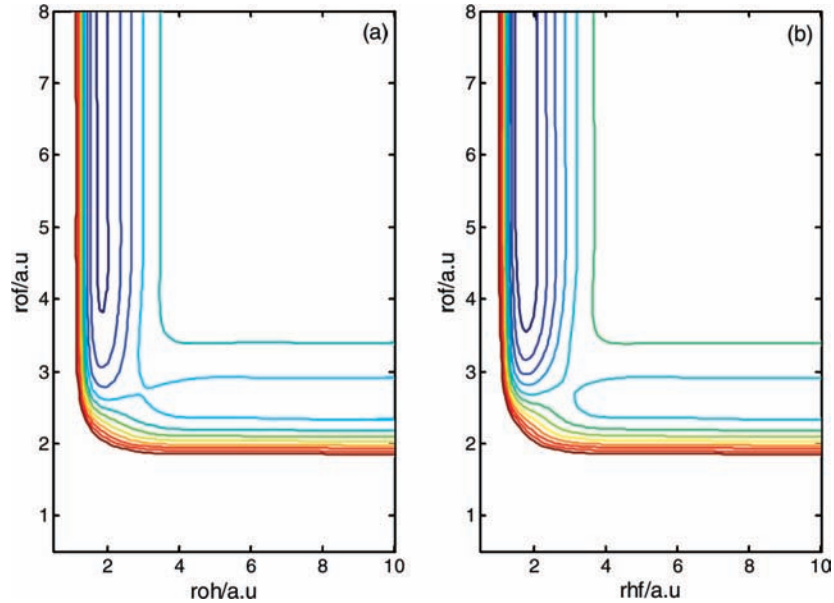

Figure 2. The $1^3A''$ PES contours at collinear structures of the H + FO reaction. (a) When H attacks the O end of the FO molecule, and the energy contours are −100, −80, −60, −40, −20, 0, 20, 40, 60, 80, 100 kcal/mol. (b) When H attacks the F end of the FO molecule, and the energy contours are −120, −100, −80, −60, −40, −10, 0, 20, 40, 60, 80, 100 kcal/mol.

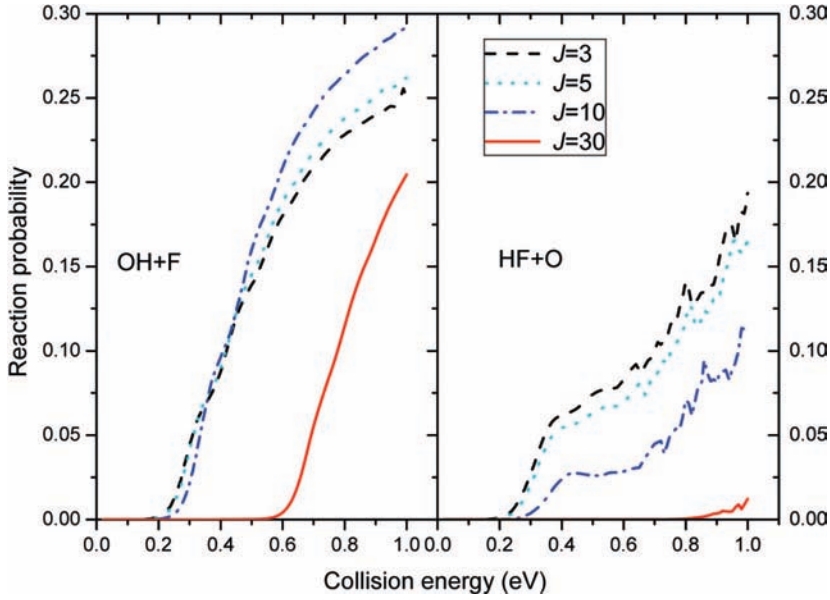

Figure 3. The calculated CS reaction probabilities as a function of collision energy for $J = 3$ (dashed line), 5 (dotted line), 10 (dash−dotted line), and 30 (solid line) for the reaction of H + FO ($v = 0, j = 0$). Left panel: OH + F product channel. Right panel: HF + O product channel.

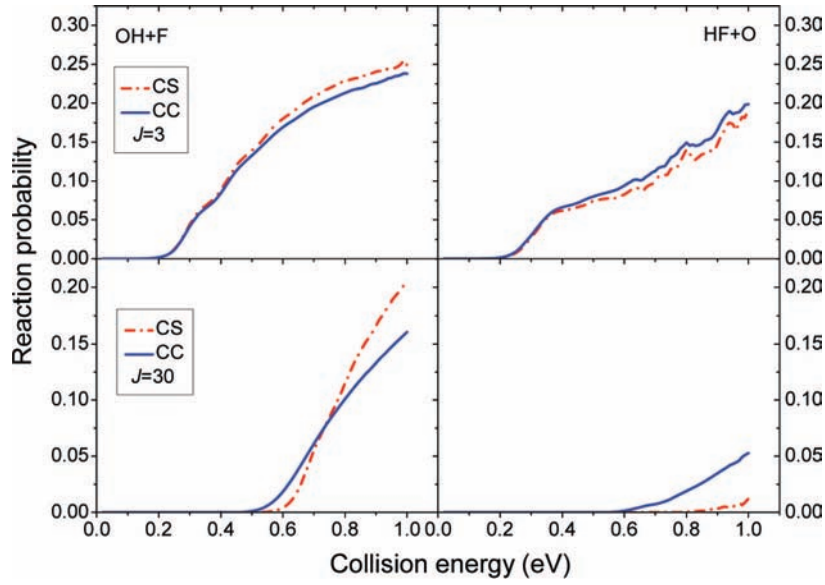

Figure 4. A comparison between the CC (solid line) and the CS (dash−dotted line) reaction probabilities for $J = 3$ and $J = 30$ for the reaction of H + FO ($v = 0, j = 0$).

the number of the grid points in the r direction (and thus the number of the vibrational basis functions) can greatly influence the calculated reaction probabilities. This can be illustrated by comparing Figure 1 with Figure 5 where the $J = 0$ reaction probabilities, calculated also from the quantum scattering calculations but with a smaller number of 120 and 90 for the grid points in the r direction and for the vibrational basis functions, respectively, are plotted as a function of the collision energies. Clearly, the unconverged $J = 0$ reaction probabilities are significantly different from those converged ones in that the unconverged results are resonance-dominated and lack an overall increasing trend in the energy-dependent behavior. Such differences reflect the significant mass effect in the reaction dynamics caused by the heavy diatomic reactant FO. The phenomena that we observed here might be one of the possible reasons for the differences in the $J = 0$ reaction probabilities between the present and the previous[6] QM scattering studies.

The batches of 25 000 trajectories are also running on the ground triplet surface to generate the $J = 0$ reaction probabilities of both product channels at a number of collision energies 0.2, 0.25, 0.3, 0.35, 0.4, 0.45, 0.5, 0.55, 0.6, 0.65, 0.7, 0.75, 0.8, 0.85, 0.9, 0.95, and 1.0 eV. The corresponding results, presented also in Figure 1, can be compared to the quantum $J = 0$ reaction probabilities. Here, we see that the reaction threshold of QCT results is almost the same as that of the quantum results, suggesting that the quantum effects such as the tunneling effect, and the effect of zero point energy, have negligible influence on the reaction dynamics of both product channels. The values of the QCT reaction probabilities are found to be close to the quantum ones in OH + F, while they are slightly smaller or larger than the quantum ones in HF + O. Moreover, the QCT calculations well reproduced the quantum energy-dependent behavior for both product channels with a clearly increasing trend. Thus, comparison of the QCT $J = 0$ reaction probabilities to the quantum results has proved that the QCT method can produce reliable dynamical quantities for the title reaction system. The validity of the QCT calculations has also been proved in a previous study of F + OH reaction on the ground

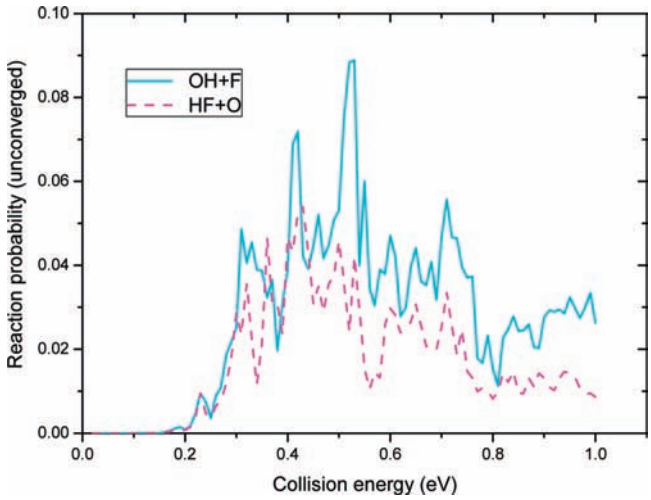

Figure 5. Unconverged quantum reaction probabilities as a function of collision energy for $J = 0$, calculated from the quantum scattering calculations using a smaller grid number of 120 in the r direction and a smaller number of 90 for the vibrational basis functions. The solid and dashed lines represent the OH + F and HF + O channels, respectively.

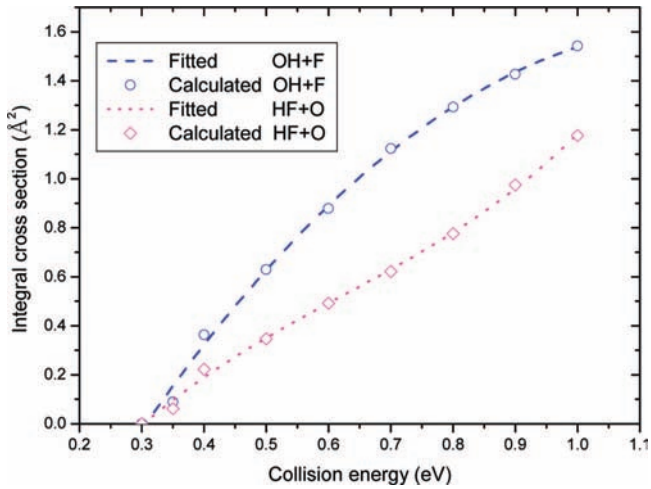

Figure 6. The calculated integral cross sections as a function of collision energy for the reaction of H + FO ($v = 0, j = 0$). The "○" and "◇" are the QCT results for OH + F and HF + O, respectively. The dashed and dotted lines are the corresponding results generated by a three-order polynomial fitting procedure.

$^1A'$ potential surface,[12] and combined with what we have found here, we presumably can say that the QCT method provides an appropriate way to study this heavy system with computational efficiency and accuracy, just as the cases in many systems.[33] In Figure 6, we further present the QCT integral cross sections as a function of collision energies for both product channels in the H + OF ($v = 0, j = 0$) reaction at collision energies 0.3, 0.35, 0.4, 0.5, 0.6, 0.7, 0.8. 0.9, and 1.0 eV. The "○" and the "◇" denote the results for OH + F and HF + O, respectively. Similar to the $J = 0$ reaction probabilities, the QCT integral cross sections of the two products exhibit a reaction threshold around the collision energy of 0.3 eV, with an increasing trend over the whole investigated energy range. The features shown here in the reaction probabilities and the integral cross sections predicted a dominant role of the early energy barrier in mediating the underlying reaction mechanisms. In addition, the larger cross sections of the OH + F channel than of HF + O indicate that formation of the former product is much easier than that of the latter in this reactive system.

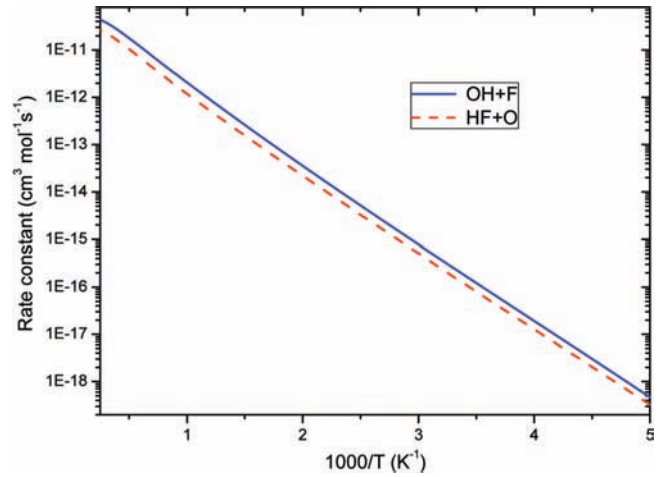

Figure 7. Arrhenius plot of the rate constants calculated by a Boltzmann averaging over the fitted integral cross sections. The solid and dashed lines denote the OH + F and HF + O channels, respectively.

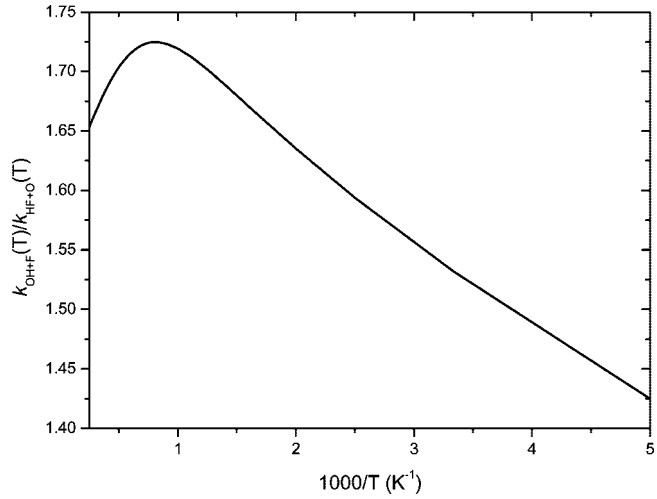

Figure 8. The branch ratio of product OH + F to product HF + O calculated from the corresponding rate constants.

Figure 6 also shows the integral cross sections obtained through a three-order polynomial fitting procedure, and the dashed and the dotted lines represent the corresponding results for the OH + F and HF + O products, respectively. The rate constants $k(T)$ deduced from the fitted cross sections by using eq 2.7 and the product branch ratio defined as $k_{OH+F}(T)/k_{HF+O}(T)$ are presented, in Figure 7 and Figure 8, over a temperature range of 200−4000 K. The product branch ratio first exhibits an increase trend with increasing temperature and reaches a maximum value of ~1.7 at 2000 K, and after that it illustrates a decreasing trend with temperature. Over the whole temperature range, the calculated branch ratio is always larger than 1.4, predicting that formation of OH product is favored over the HF product in the reaction mechanism. However, no measurements of the rate constants for formation of both products have been reported previously, which makes it unfeasible for a direct comparison of the present study with experimental measurements.

4. Conclusion

A comparative study of the H + FO reaction has been performed by simultaneously carrying out a time-dependent wave packet calculation and a QCT calculation on the ground triplet $^3A''$ surface. The $J = 0$ reaction probabilities produced

from the QCT method are compared well to the quantum results and thus validate the use of the QCT method for the reaction system. No resonance structures have been observed in both the CS quantum reaction probabilities with $J = 0$, 3, 5, 10, and 30 and the QCT $J = 0$ reaction probabilities of the OH + F product channel, while there are some oscillations in the corresponding quantum reaction probabilities of the HF + O ones. Comparison of the CS reaction probabilities with the CC ones for $J = 3$ and $J = 30$ has revealed a significant role of Coriolis coupling effects in the quantum scattering calculations of the heavy H + FO reaction. Also, no obvious resonance structure can be seen in the QCT integral cross sections. These calculated integral cross sections, and the subsequent rate constants calculated by a Boltzmann averaging over the fitted integral cross sections, as well as the branch ratio of product OH to HF, have predicted a favorable formation of the OH + F channel over the HF + O channel in the underlying reaction mechanism that is dominantly mediated by the early energy barrier in the title reactive system.

Acknowledgment. This work was supported by NSFC (10874096, 20773071) and QDUF (063-06300510).

References and Notes

(1) Gómez-Carrasco, S.; González-Sánchez, L.; Aguado, A.; Paniagua, M.; Roncero, O.; Hernández, M. L.; Alvariño, J. M. *Chem. Phys. Lett.* **2004**, *383*, 25.

(2) Gómez-Carrasco, S.; González-Sánchez, L.; Aguado, A.; Roncero, O.; Alvariño, J. M.; Hernández, M. L.; Paniagua, M. *J. Chem. Phys.* **2004**, *121*, 4605.

(3) González-Sánchez, L.; Gómez-Carrasco, S.; Aguado, A.; Paniagua, M.; Hernández, M. L.; Alvariño, J. M.; Roncero, O. *Mol. Phys.* **2004**, *102*, 2381.

(4) Gómez-Carrasco, S.; Roncero, O. *J. Chem. Phys.* **2006**, *125*, 054102.

(5) González-Sánchez, L.; Gómez-Carrasco, S.; Aguado, A.; Paniagua, M.; Hernández, M. L.; Alvariño, J. M.; Roncero, O. *J. Chem. Phys.* **2004**, *121*, 309.

(6) Gogtas, F. *J. Comput. Chem.* **2008**, *29*, 1889.

(7) Gómez-Carrasco, S.; Roncero, O.; González-Sánchez, L.; Hernández, M. L.; Alvariño, J. M.; Paniagua, M.; Aguado, A. *J. Chem. Phys.* **2005**, *123*, 114310.

(8) Han, K. L.; He, G. Z. *J. Photochem. Photobiol., C: Photochem. Rev.* **2007**, *8*, 55.

(9) Hu, J.; Han, K. L.; He, G. Z. *Phys. Rev. Lett.* **2007**, *95*, 123001.

(10) Gómez-Carrasco, S.; Aguado, A.; Paniagua, M.; Roncero, O. *J. Chem. Phys.* **2006**, *125*, 164321.

(11) Gómez-Carrasco, S.; Aguado, A.; Paniagua, M.; Roncero, O. *J. Photochem. Photobiol., A* **2007**, *190*, 145.

(12) Gómez-Carrasco, S.; Hernández, M. L.; Alvariño, J. M. *Chem. Phys. Lett.* **2007**, *435*, 188.

(13) Zhang, J. Z. H.; Dai, J. Q.; Zhu, W. *J. Phys. Chem. A* **1997**, *101*, 2746.

(14) Zhang, J. Z. H. *Theory and Application of Quantum Molecular Dynamics*; World Scientific: Singapore, 1999.

(15) Xie, T. X.; Zhang, Y.; Zhao, M. Y.; Han, K. L. *Phys. Chem. Chem. Phys.* **2003**, *5*, 2034.

(16) Yang, B. H.; Gao, H. T.; Han, K. L.; Zhang, J. Z. H. *J. Chem. Phys.* **2000**, *113*, 1434.

(17) Fleck, J. A., Jr.; Morris, J. R.; Feit, M. D. *Appl. Phys.* **1976**, *10*, 129.

(18) Nussbaumcr, H. J. *Fast Fourier Transform and Convolution Algorithms*, 2nd ed.; Springer Verlag: Berlin, 1982.

(19) Light, J. C.; Hamilton, I. P.; Lill, J. V. *J. Chem. Phys.* **1985**, *82*, 1400.

(20) Echave, J.; Clary, D. C. *Chem. Phys. Lett.* **1992**, *190*, 225.

(21) Chu, T. S.; Han, K. L. *Phys. Chem. Chem. Phys.* **2008**, *10*, 2431.

(22) Han, K. L.; Zheng, X. G.; Sun, B. F.; He, G. Z.; Zhang, R. Q. *Chem. Phys. Lett.* **1991**, *181*, 474.

(23) Han, K. L.; He, G. Z.; Lou, N. Q. *J. Chem. Phys.* **1996**, *105*, 8699.

(24) Han, K. L.; He, G. Z.; Lou, N. Q. *Chin. J. Chem. Phys.* **1989**, *2*, 323.

(25) Wang, M. L.; Han, K. L.; Zhan, J. P.; Huang, J. H.; He, G. Z. *Chem. Phys.* **1998**, *236*, 387.

(26) Wang, M. L.; Han, K. L.; Cong, S. L.; He, G. Z.; Lou, N. Q. *Chem. Phys.* **1998**, *238*, 481.

(27) Wang, M. L.; Han, K. L.; He, G. Z.; Lou, N. Q. *Chem. Phys. Lett.* **1998**, *284*, 200.

(28) Wang, M. L.; Han, K. L.; Zhan, J. P.; Wu, V. W. K.; He, G. Z.; Lou, N. Q. *Chem. Phys. Lett.* **1997**, *278*, 307.

(29) Wang, M. L.; Han, K. L.; He, G. Z. *J. Chem. Phys.* **1998**, *109*, 5446.

(30) Wang, M. L.; Han, K. L.; He, G. Z. *J. Phys. Chem. A* **1998**, *102*, 10204.

(31) Zhan, J. P.; Yang, H. P.; Han, K. L.; Deng, W. Q.; He, G. Z.; Lou, N. Q. *J. Phys. Chem. A* **1997**, *101*, 7486.

(32) Zhang, X.; Han, K. L. *Int. J. Quantum Chem.* **2006**, *106*, 1815.

(33) Ju, L. P.; Han, K. L.; Zhang, J. Z. H. *J. Comput. Chem.* **2009**, *30*, 305.

JP9003505